Effect of Aggregate and Fiber on High Temperature Performance of Ultra-High Performance Concrete

Min Xiao [1,a*], Jianqin Li [2,b], Fucai Liu [1,c], Hui Wang [2,d], Yifei Jiao [3,e]

[1]Guangdong Gaiteqi New Materials Technology Co., Ltd., Qingyuan 511600,China
[2]State Grid Economics and Technological Research Institute, Beijing 102209, China
[3]State Grid Sichuan Economic Research Institute, Chengdu 610000, China

[a]MinXiaogaiteqi@163.com, [b]lijianqin328@sina.com,
[c]jamesliu518@126.com, [d]wanghui@chinasperi.sgcc.com.cn,
[e]yifeijiao@hotmail.com
[*]Corresponding author

Abstract. This study examines the high-temperature behavior of ultra-high-performance concrete (UHPC) formulated with aluminate cement and various fiber and aggregate combinations. Key performance metrics, including compressive strength, mass loss, hydration characteristics, porosity, and microstructural changes, were evaluated across a temperature range of 200°C to 1000°C. The developed aluminate cement-based UHPC exhibited stable strength development over time. Under high-temperature exposure, UHPC containing sintered bauxite sand demonstrated superior resistance to surface cracking and lower mass loss than UHPC with quartz sand. Compressive strength increased at 200°C due to continued hydration and crystallization but declined significantly at higher temperatures due to dehydration and structural cracking. XRD and DSC analyses identified temperature-dependent phase transformations, leading to mass loss and strength reduction. SEM and porosity analyses revealed microstructural changes, including fiber degradation and pore expansion, particularly beyond 800°C. The results indicate that UHPC formulations combining both sintered bauxite sand and quartz sand with steel and PVA fibers exhibit improved high-temperature resistance.

Keywords: High temperature performance, UHPC; Compressive strength; Aluminate cement Sintered bauxite sand, quartz sand, steel fiber, PVA fibers

1 Introduction

In response to higher performance requirements on concrete materials, ultra-high-performance concrete (UHPC) has emerged, offering exceptional strength, durability, and toughness [1,2]. Currently, UHPC is widely applied in fields such as high-rise buildings [3], high-corrosion-resistance structures [4], and protective structures against explosions [5] and radiation [6].

W. Nie et al. (eds.), *Proceedings of the 2024 6th International Conference on Hydraulic, Civil and Construction Engineering (HCCE 2024)*, Atlantis Highlights in Engineering 37,
https://doi.org/10.2991/978-94-6463-726-7_42

In the power sector, ultra-high voltage converter stations are vital for direct current transmission systems. The valve hall, which houses key equipment like converter valves, has bushing openings on its firewall that pose structural vulnerabilities. Transformers in operation contain large volumes of insulating oil, creating significant fire and explosion risks during internal faults, with temperatures potentially exceeding 1000°C within 30 minutes. Current sealing systems, such as fireproof boards and blast doors, fail to fully resist explosion impacts. This highlights the urgent need for a lightweight, high-performance sealing material with superior resistance to high temperatures and explosions. UHPC, enhanced with steel fibers for added thermal resistance, offers a promising solution for these applications.

While UHPC improve mechanical performance, they also increase its susceptibility to strength loss at high temperatures [7,8]. There were plenty of studies carried out to investigate the high-temperature performance of the UHPC. Yang et al. [9] found that blending 1% steel fibers with 2% polypropylene fibers effectively suppressed spalling of UHPC at high temperatures. Peng et al. [10] observed that UHPC with coarse aggregates exhibited better high-temperature resistance. Wu et al. [11] reported that adding 0.4% polypropylene fibers reduced early-stage spalling of UHPC. Besides, Yang et al. [12] also found that UHPC specimens without steel fibers suffered severer spalling at high temperature.

The poor high-temperature performance of conventional UHPC is largely due to the presence of Portland cement in its mix. The primary hydration products of Portland cement—calcium hydroxide and calcium silicate hydrate gel—become unstable at elevated temperatures, resulting in reduced thermal performance [13]. To overcome this limitation, aluminate cement offers a promising alternative. Unlike Portland cement, aluminate cement does not produce calcium hydroxide, minimizing stress from dehydration at high temperatures. Additionally, calcium aluminate in aluminate cement generates reactive alumina when heated, which reacts with refractory aggregates to form high-melting-point minerals[14]. This suggests that replacing Portland cement with aluminate cement could significantly improve UHPC's fire resistance. Despite its potential, research on the high-temperature behavior of aluminate cement-based UHPC remains limited, necessitating further investigation.

This study investigates the high-temperature performance of aluminate cement-based UHPC. The effects of fiber and aggregate types on UHPC's appearance, mass loss, mechanical performance, and hydration are analyzed at elevated temperatures. Microstructural analyses were performed to examine microscale mechanisms underlying the performance of aluminate cement-based UHPC, providing theoretical and experimental insights to support its application in high-temperature-resistant designs.

2 Materials and Methods

2.1 Materials and Mix Proportions

The cement used in this study is CA50-I grade aluminate cement. The supplementary admixture consisted primarily of silica fume and ground granulated blast furnace slag

(GGBFS), with a 28-day activity index 110% and a water demand ratio 100%. The water reducer is a polycarboxylate-based superplasticizer, which achieves a water reduction rate of 30%. Quartz sand had a fineness modulus of 2.2. Sintered bauxite sand had a fineness modulus of 2.9 and an alumina content over 75%. Tap water was used. The steel fibers are end-hooked type 304 stainless steel fibers with a length of 14 mm and a diameter of 0.2 mm. Polyvinyl alcohol (PVA) fibers had a length of 12 mm, a diameter of 0.04 mm, and a tensile strength of 900 MPa. To investigate the effect of different aggregate and fibers, five mix proportions were designed and prepared, as shown in **Table 1**. Specimens S1F1, S2F1, and S3F1 were designed to investigate three aggregate combinations: only sintered bauxite sand, only quartz sand, and a mix of sintered bauxite sand and quartz sand, respectively. Similarly, specimens S3F1, S3F2, and S3F3 explored three fiber combinations: both PVA and steel fibers, only steel fibers, and only PVA fibers, respectively.

Table 1. Mix proportions for aluminate cement-based UHPC (kg/m^3).

ID	Cement	Supplementary admixture	Sintered bauxite sand	Quartz sand	Water	Water reducer	Steel fiber	PVA fiber
S1F1	500	445	1040	0	140	40	120	1.5
S2F1	500	445	0	1040	140	40	120	1.5
S3F1	500	445	520	520	140	40	120	1.5
S3F2	500	445	520	520	140	40	120	0
S3F3	500	445	520	520	140	40	0	1.5

2.2 Sample Preparation and Testing

Samples were prepared using an HJS-100 twin-shaft concrete mixer. The fine aggregate and fibers were first stirred for 2 mins. Cement and admixtures were then added and mixed for an additional 2 mins. Subsequently, water and a water-reducing agent were incorporated, and the mixture was stirred for a further 8 minutes, resulting in a total mixing time of 12 mins. Cubic samples measuring 100 × 100 × 100 mm^3 were cast. The cast UHPC samples underwent a 24-hour curing period with film-covered, moisture-retained conditions before demolding. Following this, they were placed in a far-infrared dry heat curing chamber for high-temperature curing. The temperature was gradually raised from room temperature to 85°C at a rate of 15°C per hour and maintained at 85°C for 48 hours. The specimens were then cooled to room temperature at a rate not exceeding 15°C per hour and subsequently stored at room temperature until testing. Compressive strength tests were conducted in accordance with the Chinese standard GB/T 31387-2015 [15]. To assess the strength development, compressive strength was measured at 7, 90, 180, and 270 days after casting.

As potential fire exposure in the power sector can reach up to 1000°C, this study investigated the performance of UHPC at five target temperatures: 200°C, 400°C, 600°C, 800°C, and 1000°C. Specimens were heated in a box furnace following the heating curve shown in **Fig. 1**, with a controlled heating rate of 20°C per minute. Once the target temperature was reached, specimens were exposed at that temperature

for 3 hours, after which the furnace was turned off, and the door was opened to allow natural cooling. After cooling to room temperature, the compressive strength of the specimens was measured according to the Chinese standard GB/T 31387-2015 [15] to evaluate the effects of high-temperature exposure. The mass of each specimen was recorded using an electronic scale before and after high-temperature treatment to calculate the mass loss rate. All tests were conducted at room temperature.

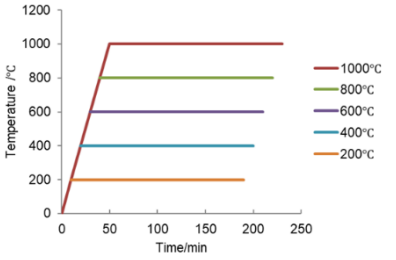

Fig. 1. Heating curve for high temperature testing

Microscopic analyses were conducted to examine the microstructural characteristics of the specimens. Following the compressive strength tests, samples were extracted for scanning electron microscopy (SEM) imaging and porosity analysis. These samples were promptly placed in plastic bottles containing anhydrous ethanol to halt hydration, sealed, and stored in a cool, dry environment for subsequent examination. The microstructure was analyzed using a HITACHI-SU8220 ultra-high-resolution field-emission SEM, following the manufacturer's operational guidelines. Porosity and pore distribution were measured using a Micromeritics AutoPore IV 9500 mercury intrusion porosimeter, adhering to the instrument's user instructions. Furthermore, powdered specimens were subjected to thermal and phase analysis using a Rigaku-SmartLab SE multifunctional X-ray diffractometer (XRD) and a TA Discovery TGA 550 thermogravimetric analyzer (TG-DSC), adhering to the instrument's user instructions. These analyses provided comprehensive insights into the microstructural and thermal behavior of the UHPC specimens.

3 Results and Discussion

3.1 Compressive Strength Development Over Time

Fig. 2 presents the compressive strength of aluminate cement-based UHPC at different curing ages. The UHPC specimen containing only quartz sand (S2F1) exhibited higher compressive strength compared to the specimen with only sintered bauxite sand (S1F1). Additionally, the specimen reinforced solely with steel fibers (S3F2) demonstrated superior compressive strength compared to the specimen reinforced with PVA fibers (S3F3). As observed, specimens subjected to 48 hours of curing at 85°C, followed by natural curing, exhibited a gradual increase in compressive strength over time. The compressive strength of all UHPC specimens at 270 days was

5–10% higher than that at 7 days, with no indications of strength retrogression. This stability in strength is largely attributed to the reaction between silica fume and slag in the supplementary admixture with aluminate cement, leading to the formation of stable C_2ASH_8 compounds. These compounds modify the hydration pathway of aluminate cement, effectively preventing strength retrogression associated with the crystalline phase transformation of aluminate cement at later stages. Additionally, a reduced water-cement ratio further contributes to slowing down the rate of crystalline transformation in aluminate cement concrete. Early high-temperature curing also facilitates the formation of C_3AH_6, promoting stable and sustained high strength over time[16].

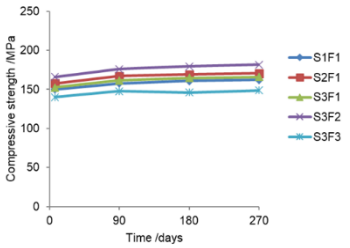

Fig. 2. Strength development of the aluminate cement-based UHPC

3.2 Appearance after High Temperature Exposure

Table 2 summarizes the appearance (specifically, the presence of cracks) of UHPC samples before and after heat treatment at various temperatures. UHPC specimens containing only quartz sand as the aggregate (S2F1) began to exhibit surface cracks at 600°C, which is a lower onset temperature compared to specimens with 50% sintered bauxite aggregate (S3F1, S3F2, S3F3) and those with only sintered bauxite aggregate (S1F1). These results indicate that sintered bauxite provides superior performance in enhancing the high-temperature resistance of UHPC compared to quartz sand.

All specimens displayed similar behavior as the temperature increased. The appearance of specimen S3F1, representative of this trend, is shown in **Fig. 3**. As illustrated in **Fig. 3** (a-c), specimens subjected to temperatures below 400°C showed no significant changes in color or surface cracking. However, as shown in **Fig. 3**(d-f), exposure to temperatures above 600°C led to gradual darkening and yellowish discoloration. Surface cracks became noticeable at temperatures exceeding 800°C (see **Fig. 3** (e)), with further crack development observed after exposure to 1000°C.

Table 2. Summary of appearance of all UHPC samples before and after heat treatment

ID	Before	After 200°C	After 400°C	After 600°C	After 800°C	After 1000°C
S1F1	No Cracking	No Cracking	No Cracking	No Cracking	Cracking	Cracking
S2F1	No Cracking	No Cracking	No Cracking	Cracking	Cracking	Cracking
S3F1	No Cracking	No Cracking	No Cracking	No Cracking	Cracking	Cracking
S3F2	No Cracking	No Cracking	No Cracking	No Cracking	Cracking	Cracking
S3F3	No Cracking	No Cracking	No Cracking	No Cracking	Cracking	Cracking

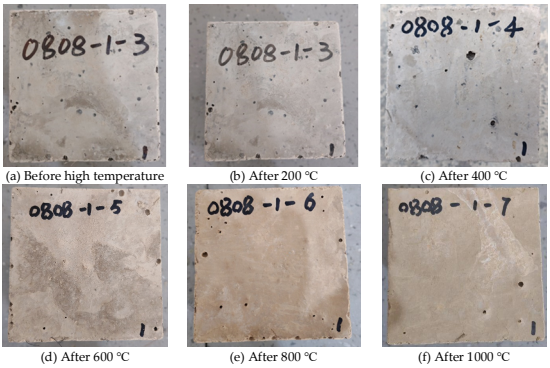

(a) Before high temperature (b) After 200 ℃ (c) After 400 ℃

(d) After 600 ℃ (e) After 800 ℃ (f) After 1000 ℃

Fig. 3. Appearance of the UHPC sample S3F1 before and after heat treatment

3.3 Mass Loss after High Temperature Exposure

Fig. 4 shows the mass loss of UHPC samples after exposure to various temperatures. As illustrated, the mass loss increased with rising temperature. Concrete undergoes mass loss at elevated temperatures due to factors such as moisture evaporation, dehydration and decomposition of hydration products, and phase transformations within hydration products and aggregates. Consequently, the mass loss at high temperatures provides insight into changes occurring within the internal structure of concrete.

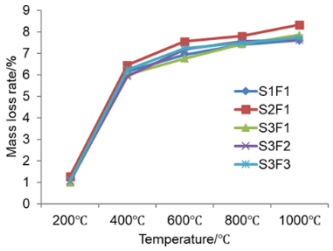

Fig. 4. Mass loss of all UHPC samples before and after high temperature treatment

All samples displayed a similar trend in mass loss. The specimen with only quartz sand showed higher mass loss than the others, aligning with the appearance observations described in the previous section. This finding further confirms that sintered bauxite sand enhances the high-temperature performance of UHPC more effectively than quartz sand. Overall, the effects of aggregate type and fiber addition on mass loss were minor. Notably, as the temperature increased from 200°C to 400°C, the mass loss rate of all samples rose sharply from about 1% to about 6%, indicating a 5% increase. This pronounced rise in mass loss suggests that significant transformations within the hardened cement matrix likely occur within this temperature range, leading to the formation of volatile compounds that evaporate at high temperatures.

3.4 Compressive Strength after High Temperature Exposure

Fig. 5 presents the compressive strength of UHPC samples following exposure to various high temperatures. After high-temperature curing, the compressive strength of the aluminate cement-based UHPC at the room temperature was generally around 150 MPa. As shown in **Fig. 5**, the compressive strength of the UHPC initially increases with temperature, reaching a peak at 200°C, before decreasing at higher temperatures. At 200°C, further hydration and crystallization of the aluminate cement occur, with hydration products filling internal pores and enhancing UHPC strength. Samples S3F1 and S1F1 exhibited the highest strength increases, rising by 30–34%, followed by a 20% increase in S3F3, while Samples S3F2 and S2F1 showed only an 11% increase. However, as temperatures exceeded 200°C, compressive strength began to decline, dropping to approximately 50% of the initial strength at 1000°C.

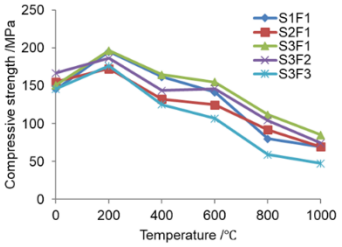

Fig. 5. Compressive strength of UHPC samples before and after high temperature treatment

When comparing different aggregate types, Sample S1F1 (containing only sintered bauxite sand) retained 97% and 48% of its original strength after exposure to 600°C and 1000°C, respectively, while Sample S2F1 (containing only quartz sand) retained 85% and 45% of its original strength at the same temperatures. The slower rate of strength decline in Sample S1F1 indicates that sintered bauxite sand provides greater stability than quartz sand, particularly at temperatures up to 600°C, making it a more advantageous choice for enhancing the high-temperature performance of aluminate cement-based UHPC. Additionally, Sample S3F1, which used a combination of sintered bauxite sand and quartz sand, retained 103% and 56% of its original strength after exposure to 600°C and 1000°C, respectively, indicating a coupling effect of both aggregates that provides better performance than using either aggregate alone.

Further comparisons among samples with different fiber types reveal notable differences. Sample S3F3, containing only PVA fibers, retained 86%, 73%, 40%, and 33% of its original strength after exposure to 400°C, 600°C, 800°C, and 1000°C, respectively. In contrast, Sample S3F2, containing only steel fibers, retained 86%, 88%, 62%, and 45% of its strength at these temperatures. The slower rate of strength decline in Sample S3F2 suggests that steel fibers are more effective than PVA fibers at improving high-temperature performance. Moreover, Sample S3F1, incorporating both steel and PVA fibers, retained 109%, 103%, 74%, and 56% of its strength after exposure to 400°C, 600°C, 800°C, and 1000°C, respectively, indicating an even

slower rate of decline compared to Sample S3F2. This suggests a synergistic effect between steel and PVA fibers, resulting in superior high-temperature performance.

3.5 Hydration Analysis

To identify the hydration products in aluminate cement-based UHPC, XRD and TG analyses were conducted on UHPC samples exposed to various high temperatures, with sample S3F1 selected for representative purposes. The XRD results are displayed in **Fig. 6**, while the differential scanning calorimetry (DSC) curve from the TG analysis is shown in **Fig. 7.**

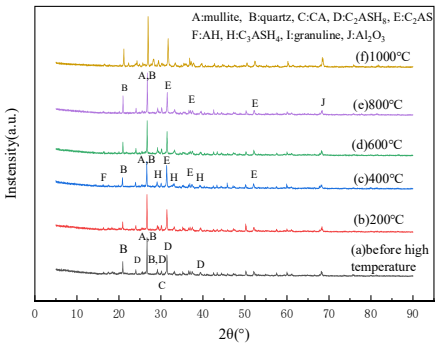

Fig. 6. XRD results of aluminate cement-based UHPC sample S3F1

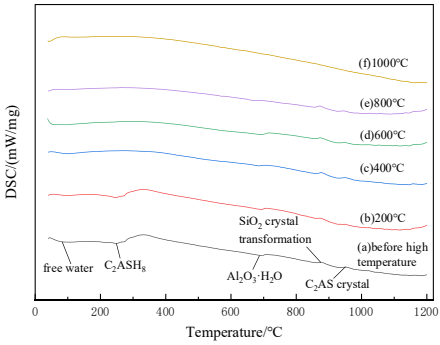

Fig. 7. DSC of aluminate cement-based UHPC sample S3F1

According to the XRD results in **Fig. 6**, the primary hydration product observed in the sample prior to high-temperature treatment was C_2ASH_8. Generally, calcium aluminate in aluminate cement initially hydrates to form CAH_{10} and C_2AH_8. However, when the ambient temperature exceeds 30°C, these products transform into C_3AH_6. The incorporation of silica fume and slag reacts with these hydration products, stabilizing C_2ASH_8 as the main compound. This explains the presence of C_2ASH_8 and the absence of CAH_{10}, C_2AH_8, and C_3AH_6 in the sample. As the exposure temperature

increased, C_2ASH_8 disappeared, and C_2AS began to form. This transition occurs because C_2ASH_8 dehydrates at temperatures above 200°C, converting into C_2AS [17]. The initial phase of this transformation leads to a loosening of the UHPC structure and a reduction in strength. In the subsequent phase, the continuous crystallization of C_2AS at elevated temperatures results in volume expansion, further damaging the UHPC structure and causing a notable decline in strength. Additionally, under high-temperature conditions with moisture, C_2ASH_8 may decompose into boehmite ($Al_2O_3 \cdot H_2O$) and hydrated garnet C_3ASH_4 ($3CaO \cdot Al_2O_3 \cdot SiO_2 \cdot 4H_2O$). The presence of Al_2O_3 in the XRD pattern for samples exposed to temperatures above 800°C indicates this decomposition. The dehydration and decomposition of C_2ASH_8 contribute significantly to the observed strength and mass losses after high-temperature exposure.

As observed in the DSC curves in **Fig. 7**, an endothermic peak around 100°C in the sample before high-temperature treatment indicates the evaporation of free water. The endothermic peak at approximately 248°C corresponds to the dehydration of C_2ASH_8 into C_2AS. An endothermic peak around 690°C signifies the dehydration of boehmite ($Al_2O_3 \cdot H_2O$), resulting in γ-Al_2O_3 formation. The exothermic peak at 870°C corresponds to the transformation of quartz to cristobalite, a process involving crystal structure reconstruction. This transformation causes approximately 16% expansion in the quartz volume, leading to deformation and crack formation [18]. Another exothermic peak at 949.3°C is associated with the crystallization of C_2AS [17], after which the crystal structure of C_2AS becomes more complete. Following high-temperature treatments, these endothermic and exothermic peaks disappear, indicating that all reactions and transformations associated with these temperatures were completed during heat treatment. The crystallization of C_2AS after 949.3°C exhibits anisotropic expansion, differing from the thermal expansion rates of steel fibers and hydration products. This mismatch leads to separation between the steel fibers and cement matrix, resulting in cracking and strength reduction after high-temperature treatment at 1000°C. Overall, the observations from the DSC curves align well with those from the XRD patterns.

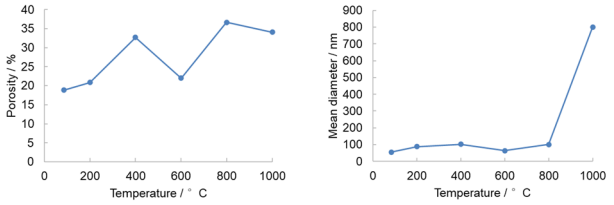

(a) Porosity (b) Mean pore diameter

Fig. 8. Porosity analysis of aluminate cement-based UHPC sample S3F1

3.6 Porosity and Microscope Analysis

The porosity of the UHPC sample S3F1 is presented in **Fig. 8**. As the exposure temperature increases to 400°C, both porosity and mean pore diameter gradually increase,

primarily due to the evaporation of free water and dehydration of C_2ASH_8. From 400°C to 600°C, continuous crystallization of C_2AS causes expansion, reducing porosity and partially compensating for strength loss. This aligns with the observations in **Fig. 5,** where the strength loss between 400°C and 600°C is slight. As the temperature rises from 600°C to 800°C, the dehydration of boehmite ($Al_2O_3 \cdot H_2O$) results in increased porosity and larger pore diameters. When the exposure temperature reaches 1000°C, expansion due to C_2AS crystallization leads to cracking, significantly increasing pore diameters. Additionally, the transformation of quartz to cristobalite at this stage contributes to expansion, which reduces porosity to some extent.

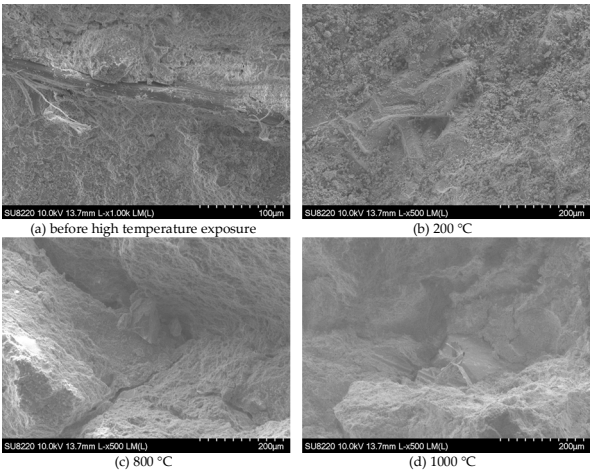

Fig. 9. Scanning electron microscope of aluminate cement-based UHPC sample S3F1

The SEM images of the UHPC sample S3F1 after high-temperature exposure are shown in **Fig. 9**. Before high-temperature treatment, a tight bond between the aggregate and fiber is evident (see **Fig. 9**(a)), along with a dense matrix structure, which contributes to the high strength of UHPC. After exposure to 200°C, the SEM image (see **Fig. 9**(b)) also reveals a highly compact matrix between the paste and aggregates. This is due to further crystallization of hydration products at 200°C, which enhances microstructural density and results in a notable increase in strength. After exposure to 800°C, SEM images (see **Fig. 9**(c)) reveal the formation of cracks between the paste and aggregate, as well as within the paste itself. These cracks are likely caused by the decomposition of PVA fibers at high temperatures, which enlarges the pores in the UHPC matrix. The degraded PVA fibers and increased porosity together result in a significant reduction in UHPC strength and noticeable mass loss. Following exposure to 1000°C, these phenomena become more pronounced. The SEM image (see **Fig. 9**(d) shows extensive internal cracking, fiber detachment, and a loosening of the UHPC structure, all of which contribute to a marked decline in both strength and mass.

4 Conclusion

This study investigated the effects of high-temperature on compressive strength, mass loss, hydration, and microstructure of aluminate cement-based UHPC with various fiber and aggregate combinations. The key findings are summarized as follows:

- The developed UHPC demonstrated increasing compressive strength over time. This stability is primarily attributed to the formation of stable C_2ASH_8 through the reaction of silica fume and slag with aluminate cement.
- UHPC samples with sintered bauxite sand exhibited greater resistance to surface cracking and lower mass loss after high-temperature exposure compared to those with quartz sand.
- The compressive strength of UHPC samples increased initially, and then declined significantly due to dehydration and cracking. Samples incorporating both steel and PVA fibers, along with a blend of sintered bauxite and quartz sand, showed improved performance.
- XRD and DSC analyses identified C_2ASH_8 as the primary hydration product after high-temperature curing, with a transition to C_2AS and other phases occurring as temperature increases. This contributes to mass loss and strength reduction.
- Both porosity and mean pore diameter increased with temperature up to 400°C A temporary reduction in porosity was observed between 400°C and 600°C due to C_2AS crystallization. Above 800°C, substantial increases in porosity and pore size occurred due to structural cracking.
- SEM images revealed a dense microstructure in samples exposed to 200°C. However, temperatures exceeding 800°C caused significant internal cracking and fiber detachment, which resulted in reduced strength.

Acknowledgments

This research was funded by the State Grid Corporation of China (No. 5108-202218280A-2-317-XG)

References

1. Guo, W., Chen, B., Yang, Y., Xia, Y., Xiao, Q., Liu, S., & Wang, H. (2024). Effect of Curing Regimes and Fiber Contents on Flexural Behaviors of Milling Steel Fiber-Reinforced Ultrahigh-Performance Concrete: Experimental and Data-Driven Studies. *Journal of Materials in Civil Engineering*, *36*(7), 04024152. https://doi.org/10.1061/JMCEE7.MTENG-17429
2. Yang, Y., Yue, X., Chen, B., Yang, W., Guo, W., & Wang, H. (2024). Autogenous shrinkage and cracking of ultra-high-performance concrete with soda residue as an internal curing agent. *Materials and Structures*, *57*(10), 216. https://doi.org/10.1617/s11527-024-02499-4

3. M. AlHamaydeh, M. E. Elkafrawy, M. Kyaure, M. Elyas, & F. Uwais. (2022). Cost Effectiveness of UHPC Ductile Coupled Shear Walls for High-Rise Buildings in UAE Subjected to Seismic Loading. *2022 Advances in Science and Engineering Technology International Conferences (ASET)*, 1–6. https://doi.org/10.1109/ASET53988.2022.9734843
4. Song, Z., Li, S., Brouwers, H. J. H., & Yu, Q. (2023). Corrosion risk and corrosion-induced deterioration of ultra-high performance fiber-reinforced concrete containing initial micro-defects. *Cement and Concrete Composites*, *142*, 105208. https://doi.org/10.1016/j.cemconcomp.2023.105208
5. Xu, S., Yuan, P., Liu, J., Yu, X., Hao, Y., Hu, F., & Su, Y. (2022). Experimental and numerical investigation of G-UHPC based novel multi-layer protective slabs under contact explosions. *Engineering Failure Analysis*, *142*, 106830. https://doi.org/10.1016/j.engfailanal.2022.106830
6. Zeyad, A. M., Hakeem, I. Y., Amin, M., Tayeh, B. A., & Agwa, I. S. (2022). Effect of aggregate and fibre types on ultra-high-performance concrete designed for radiation shielding. *Journal of Building Engineering*, *58*, 104960. https://doi.org/10.1016/j.jobe.2022.104960
7. Hernández-Figueirido, D., Reig, L., Melchor-Eixea, A., Roig-Flores, M., Albero, V., Piquer, A., & Pitarch, A. M. (2024). Spalling phenomenon and fire resistance of ultrahigh-performance concrete. *Construction and Building Materials*, *443*, 137695. https://doi.org/10.1016/j.conbuildmat.2024.137695
8. Amran, M., Murali, G., Makul, N., Kurpińska, M., & Nehdi, M. L. (2023). Fire-induced spalling of ultra-high performance concrete: A systematic critical review. *Construction and Building Materials*, *373*, 130869. https://doi.org/10.1016/j.conbuildmat.2023.130869
9. Yang, T., Liu, Z., Yang, Y., & Wu, C. (2020). Experimental investigation on behavior of ultra-high performance concrete after high temperature. *Journal of Civil and Environmental Engineering*, *3*.
10. Peng, G., Yang, J., Shi, Y., Niu, X., Zhao, Y., & Shang, Y. (2017). Explosive Spalling Resistance of Ultrahigh Performance Concrete. *Journal of Building Materials*, *2*.
11. Wu, J., Guo, L., Cao, Y., & Fei, X. (2022). The Performance of Ultra-high Performance Concrete Exposed to 600 ℃ at Early Stage. *Materials Reports*, *36*(3), 20110163–20110166. https://doi.org/10.11896/cldb.20110163
12. Yang, J., & Peng, G. (2018). Influence of different types of steel fiber on explosive spalling behavior of ultra-high-performance concrete exposed to high temperature. *Acta Materiae Compositae Sinica*, *6*. https://doi.org/10.13801/j.cnki.fhclxb.20170821.009
13. Tantawy, M. (2017). Effect of high temperatures on the microstructure of cement paste. *Journal of Materials Science and Chemical Engineering*, *5*(11), 33–48.
14. Sun, H., Wang, L., & Cao, M. (2003). The test research on strength and durability of refractory concrete with high aluminum cement after a fire. *Industrial Construction*, *9*.
15. Standardization Administration of the PRC. (2015). *GB/T 31387-2015 Reactive powder concrete*.
16. Sakai, E., Sugiyama, T., Saito, T., & Daimon, M. (2010). Mechanical properties and micro-structures of calcium aluminate based ultra high strength cement. *Cement and Concrete Research*, *40*(6), 966–970. https://doi.org/10.1016/j.cemconres.2010.01.001
17. Yang, N., & Yue, W. (2000). *Handbook of Atlas of inorganic nonmetallic materials*. Wuhan University of Technology Press.
18. Zhang, C. (1996). Research on quartz ceramics. *Jiangsu Ceramics*, *2*. https://doi.org/10.16860/j.cnki.32-1251/tq.1996.02.010